The International Journal of Advanced Manufacturing Technology (2020) 110:829–840
https://doi.org/10.1007/s00170-020-05892-9

ORIGINAL ARTICLE

Utilization of ultrasonically forced pulsating water jet decaying for bone cement removal

Akash Nag[1] · Sergej Hloch[2,3] · Amit Rai Dixit[1] · Frank Pude[4]

Received: 24 April 2020 / Accepted: 9 August 2020 / Published online: 17 August 2020

Abstract

Ultrasonic pulsating water jet for non-thermal and selective removal of acrylic bone cement is studied. Variation of acoustic chamber length is used for tuning of the ultrasonic system into the resonance regime to gain maximum power transmission. The study investigates the minimal technological conditions such as nozzle traverse speed and supply water pressure required to generate disintegration grooves in bone cement mantle. It also proposes the safe standoff distance range, which is essential for its potential application during the extraction of bone cement without compromising host bone. Palacos R+G bone cement was used for the experiments. Generated groove depths were measured using MicroProf FRT and analyzed using SPIP software. Depth values showed an increasing trend with an increase in acoustic chamber length, decrease in traverse speed, and increase in supply pressure values. From the entire experimental domain, a maximum depth of 615 μm was obtained at 22-mm chamber length, 0.5-mm/s traverse speed, 10-MPa pressure, and a standoff distance of 4 mm. Brittle fractured surface features like material chipping, micro-pits, cracks, and sheared material layers were observed in the SEM images. Disintegrated debris, diameter 21–37 μm, conceived from pit diameters can be used to design a suction unit. Real-time control of the disintegration process using accelerometer sensors was shown. The results support the idea of using pulsating water jet for bone cement removal in a single blind hole. Minimal technological parameters reduce reaction force of the hand tool, allowing bone cement removal without bone fracture or perforation.

Keywords Ultrasonic resonance · Pulsating water jet · Bone cement removal · Surface morphology

Abbreviations

β	Solid–liquid contact angle [°]
ρ_1	Density of liquid [kg/m^3]
ρ_2	Density of solid [kg/m^3]
Δt	Time period [s]
c_1	Acoustic velocity of liquid [m/s]
c_2	Acoustic velocity of solid [m/s]
d	Nozzle diameter [mm]
D	Hole diameter [mm]
f_o	Operating frequency [kHz]
f_i	Initial frequency [kHz]
h	Disintegration depth [μm]
l_c	Acoustic chamber length [mm]
p	Supply water pressure [MPa]
p_i	Compressive stress [MPa]
p_s	Stagnation pressure [MPa]
P	Output power [W]
Q	Theoretical volume flow rate [L/min]
r	Radius of liquid mass [mm]
v	Traverse speed [mm/s]
v_w	Liquid velocity [m/s]
z	Standoff distance [mm]
CWJ	Continuous water jet
PWJ	Pulsating water jet

✉ Sergej Hloch
sergej.hloch@tuke.sk

[1] Indian Institute of Technology (Indian School of Mines), Dhanbad 826001, India

[2] Faculty of Manufacturing Technologies TUKE with a seat in Prešov, 08001 Prešov, Slovakia

[3] Institute of Geonics of the Czech Academy of Sciences, 70800 Ostrava-Poruba, Czech Republic

[4] Steinbeis High-Pressure Waterjet Technology Consulting Centre, 86497 Horgau, Germany

1 Introduction

Continuous water jet (CWJ) is being used for the disintegration of engineering and non-engineering material due to its cutting efficiency utilizing liquid pressures in the range of p = 400 to 600 MPa [1]. These pressures are used to increase the stagnation pressure of the continuous jets. The initial contact of the jet with the material causes damage or cracking in the brittle material due to the impact pressure [2]. Impact pressures are also observed during impingement of water droplets with solids. The initial impingement of the liquids with the solid is still explained by the water hammer phenomenon. The water pulse impacts the solid surface and induces compressive stress p_i in the solid given by Eq. 1 [3].

$$p_i = \frac{v_w \rho_1 c_1 \rho_2 c_2}{\rho_1 c_1 + \rho_2 c_2} \tag{1}$$

where v_w is the liquid impact velocity, ρ_1 and ρ_2 are densities of liquid and interacting solid, respectively, and c_1 and c_2 are acoustic velocities of liquid and solid, respectively.

After a short time interval of Δt given by Eq. 2 [4], impact pressure at the central axis of the impact reduces to stagnation pressure p_s given by Eq. 3. The second stage of impact begins when the compressibility limit of liquid deformation given by Eq. 4 is reached [5].

$$\Delta t = \frac{3rv}{2c^2} \tag{2}$$

$$p_s = \frac{1}{2}\rho v^2 \tag{3}$$

$$\frac{v}{c_1} = \sin\beta \tag{4}$$

where r is the radius of liquid mass and β is the solid–liquid contact angle.

It causes the lateral liquid to flow parallel to the solid surface, with tangential velocity approximately five times the impact velocity [6]. The interaction of the lateral flow generates shear forces on the solid surface. The local shear fractures are caused by the surface asperities of the material. Nonperiodic impingements of the droplets are observed on the turbine blades and leading edge of aircraft wings. This impingement can be used for controlled and repetitive loading of the material at a focused area which accelerates the failure mechanism and disintegration of the material. It allows to create technology of pulsating water jets operating at pressures p < 100 MPa.

For forced decaying of jets, rotary disks [7], self-resonating nozzles [8], pulsation through ultrasonic needles [9], and valve spring blocking [10] methods are used. However, certain limitations in terms of short service life of moving parts, complicated construction, and attenuation in the erosion with small change in dimension are associated with these methods of jet modulation [11, 12]. Recently, Foldyna et al. [13] developed a method of ultrasonic pulsating water jet with variable acoustic chamber length (l_c). The variation of the l_c allows to tune the resonance frequency and output power. In an acoustic chamber, an ultrasonic sonotrode periodically creates pressure fluctuations in water pressure p < 100 MPa delivered by the pump. The sonotrode generates standing waves inside the acoustic chamber. The amplitude of standing waves increases toward the nozzle exit due to its converging shape. After the nozzle exit, these pressure fluctuations change into velocity fluctuations [14]. The variations in the axial velocity cause forced decaying of the jet to form water clusters of liquid droplets [15]. The series of water pulses impinges the surface and erodes the material in different erosion regimes parametrically described by Hloch et al. [16].

The positive aspects of PWJ technology such as nonthermal [17], low reactive force (< 10 N at p = 7 MPa) [18] and selective disintegration [19] make it feasible for medical applications. One of the potential areas for utilizing PWJ can be during extraction of bone cement in revision hip arthroplasty surgeries. The procedure requires extraction of the bone cement from the femoral canal without damaging the neighboring host femur bone (Fig. 1). The currently used extraction techniques of bone cement during revision procedures involve the use of mechanical tools such as chisels, hammers, high-speed drills, and burrs [20]. These methods include risk of fracture, considerable bone loss, and longer operative time and care. Utilization of ultrasound energy [21] and delivering shockwaves through lithotripter [22] for weakening and extraction of the cement have also been reported in some in vitro studies of cement extraction. Perforation and microfractures of the surrounding bone may occur during the revision surgery. Different laser sources (Er:YAG, Nd:YAG, and CO_2) are also being used in experimental studies for the melting and disintegration of bone cement [23, 24]. The limited ablation rate, extensive carbonization, and generation of fumes are drawbacks of this method [25]. Therefore, PWJ can be hypothesized as a potential method by overcoming these limitations of the current methods with properties like cold cutting and selective disintegration. Figure 1 shows the hypothesized method of utilizing PWJ during extraction of bone cement from the femoral canal during revision hip arthroplasty procedure.

A pilot experiment for verifying the hypothesis of the selective disintegration property of the PWJ was conducted. A titanium endoprosthesis was inserted into the spongious bone structure and fixed using acrylic bone cement (Palacos R+G) to replicate the actual revision arthroplasty conditions. A single pass of PWJ with p = 20 MPa was conducted over the spongious structure, resulting in no significant visual disintegration (Fig. 2a). Next, the bone cement interface was subject to PWJ with the same technological parameters as the previous pass (Fig. 2b). Bone cement was disintegrated, resulting in

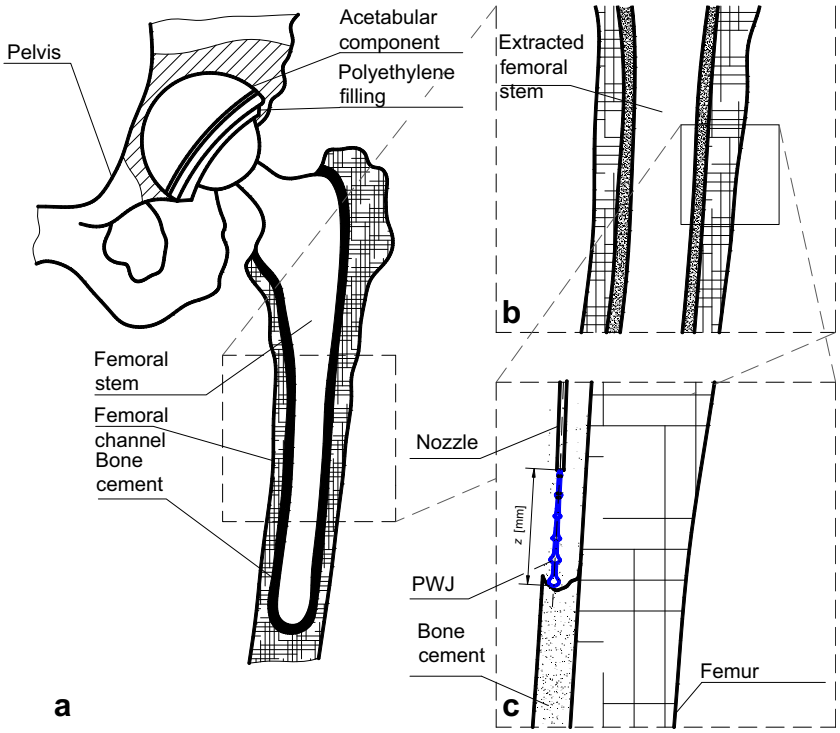

Fig. 1 Hypothesized methodology of extraction of bone cement using PWJ

the formation of a cavity between the stem and the bone. The walls of the spongious bone and endoprosthesis surface remained intact and unaffected from the impact of the PWJ during bone cement disintegration. The pilot test validates the hypothesis of selective disintegration based on physical properties of the material during PWJ disintegration.

Previous studies found in the open literature dealing with disintegration of bone cement using water jet technologies are discussed here. Honl et al. [18] carried out a parametric study on the disintegration of bone cement using CWJ and abrasive water jet (AWJ). Technovit bone cement was used to perform the experiments with a nozzle diameter of 0.3-mm pressure ranging from 20 to 120 MPa for CWJ and 20 to 60 MPa for AWJ, a traverse speed of 10 mm/min, and standoff distance of 4 mm. Visible disintegration with irregular cutting traces was observed at 40 MPa with CWJ. With AWJ, disintegration grooves with fine traces were observed for all pressure levels. Deep propagating cracks were observed, which is beneficial for cement removal during revision surgeries. Honl et al. [26] further investigated the influence of pressure (i.e., p = 30, 40, 50, 60, and 70 MPa) while disintegrating CMW3 bone cement using CWJ and AWJ. Nozzle diameter of d = 0.2 mm for CWJ and AWJ and traverse speed of v = 10 mm/min were used during the experiments. Observable grooves were formed at all pressures using CWJ. Deep cracks with a rough cutting line were observed close to the grooves. However, using AWJ,

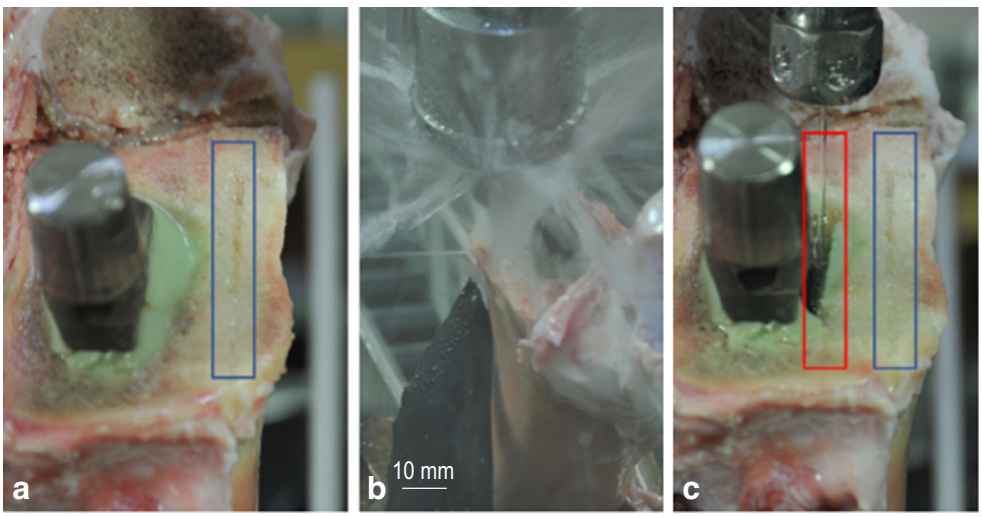

Fig. 2 Effects of pulsating water jet with 20-MPa (**a**) spongious structure—first pass (blue), (**b**) disintegration/bone cement removal from femoral channel, (**c**) removed bone cement (red) after first pass with intact bone wall

deeper grooves, 8.82 ± 0.83 mm as compared with 2.21 ± 0.24 mm at p = 60 MPa, were observed with lesser number of cracks around the periphery of the grooves. Kraaij et al. [27] disintegrated periprosthetic tissue with CWJ using jet diameters of 0.2 mm and 0.6 mm, standoff distance of 5 mm, and traverse speed of 0.5 mm/s. Water pressure of 10 and 12 MPa was required to disintegrate the tissue using a nozzle diameter of 0.2 mm; for a 0.6-mm nozzle, observable disintegration was achieved at pressures of 5 and 10 MPa. Hloch et al. [28] carried out a comparative study on disintegration of bone cement using CWJ and PWJ. Experiments were performed on Palacos R+G bone cement using a 0.7-mm circular nozzle and a 0.8-mm flat nozzle using a pressure of 8–20 MPa for PWJ. For CWJ, a pressure of 40, 80, and 120 MPa was used with a nozzle diameter of 0.1 mm. The result showed shallow grooves using CWJ whereas deeper grooves were observed with PWJ. Moreover, disintegration using a circular nozzle was deeper than using a flat nozzle at the same parametric values. Hloch et al. [29] compared the disintegration effect of PWJ on six commercially available bone cements, with pressure variation from 8 to 20 MPa using a nozzle diameter of 0.7 mm, standoff distance of 2 mm, and traverse speed of 1 mm/s. The depth of the grooves ranged between 0.5 and 2.8 mm, and no significant differences in groove depth were observed for different bone cements. Hloch et al. [30] used acoustic emission (AE) measurements to monitor the comparative disintegration process of bone cement using water and 0.9% physiological saline with PWJ. Palacos R+G bone cement was used during the experiments with a pressure ranging from 7 to 10 MPa. The results showed deeper grooves while disintegrating using 0.9% physiological saline (1.31 mm) as compared with water (1.12 mm) at the same pressure (10 MPa). An increase in volume removal rate was also observed while using 0.9% physiological saline (0.417 and 0.194 mm^3 for 0.9% physiological saline and water, respectively, at p = 10 MPa). The AE signals showed different modes of disintegration occurring during the experiments. The technological limitation with continual water jet was high pressure (p > 400 MPa) leading to increase in the volume flow rate of the liquid. PWJ solves the aforementioned problem with continuous jet.

Tuning of the resonance frequency to gain maximum power transmission given by the variation in acoustic chamber length requires proper parametric investigation. The selection of the acoustic chamber length in the past studies does not explain why and how this acoustic chamber length value was fixed for conducting the experiments. It is crucial for standoff distance investigation utilizing the vertical structure of the PWJ which allows to propose the safe standoff distance for bone cement removal.

The study aims to investigate the morphological regime of the forced decaying jet in terms of standoff distance (z), where the water hammer effect is evident during the disintegration of bone cement. Jet breakdown is fortified by the ultrasonic sonotrode depending upon its operating frequency (f_o) and output power (P), adjusted by the acoustic chamber length (l_c). The morphology of the PWJ after the nozzle exit is defined by the technological parameters such as nozzle traverse speed (v) and supply water pressure (p). The research verifies that the physical nature of the PWJ structure has potential for its utilization in safe and controlled bone cement removal without requiring a visual approach.

2 Materials and methods

Palacos R+G bone cement was used during the experiments due to its acceptance for standard use in clinical studies carried out in recent years. The bone cement was prepared in the laboratory according to the manufacturer's instructions, with necessary safety precautions. Mixing of the polymer powder and monomer liquid was done manually to obtain a dough which then solidifies within 7–8 min. The bone cement dough prepared was filled in an aluminum matrix cavity, for easy fixing to the experimental table. The compressive strength of the hardened cement was in the range of 78–80 MPa.

Experiments were performed using a high-pressure pump (Hammelmann HDP 253) with a maximum flow rate of Q = 67 L/min and maximum operating pressure of p = 160 MPa. An ABB robot (IRB 6640-180) was used to control the movement of the nozzle head, and a 0.3-mm circular nozzle was fitted at the exit of the nozzle head. The desired value of water flow rate (0.38–0.54 L/min) was adjusted using bypass valve in series to the water line between the high-pressure pump and the nozzle head. The theoretical water flow rate was calculated using Eq. 5.

$$Q = v\,A \tag{5}$$

where, $A = \frac{\pi}{4}d^2$, $v = \mu\sqrt{\frac{2p}{\rho}}$

Q = theoretical water flow rate, v = velocity of the jet, A = cross-section area of the nozzle, d = diameter of the nozzle, μ = discharge coefficient, p = supply pressure, and ρ = density of the fluid. Ultrasonic energy for the excitation of piezoelectric crystals was generated by an Ecoson WJ-UG 630-40 with a maximum power output of 800 W.

For determination of the optimal l_c, the sonotrode initial frequency was set to f_i = 21 kHz, which corresponds to the maximum excitation frequency limit of the ultrasonic generator. When powering the ultrasonic generator, the oscillating frequency would adjust itself to the operating frequency f_o with which the sonotrode vibrates depending upon the tuning of the system and flow conditions of the experimental run. The f_o and P values of the sonotrode are displayed in a hand-held device used for controlling the ultrasonic generator. The l_c was adjusted by rotating a mechanical nut attached to the

nozzle head with an increment of 2 mm, from 0 to 22 mm, and both f_o and P values for every l_c setting were noted down. At l_c = 24 mm, the P value suddenly increases > 350 W, and the oscillations stopped due to overheating of the piezoelectric crystals, determining the upper limit of l_c to 22 mm. Erosion tests for every l_c value were conducted by varying z = 2 to 20 mm followed by measurement of each disintegration groove depth (Fig. 3). The nozzle head followed a stepped trajectory with a horizontal distance of 15 mm and a step height of 2 mm. The l_c was fixed to the value at which maximum depth was achieved, and v was varied from 2 to 0.5 mm/s to observe its influence on disintegration depth. The v value was then fixed to the level which generated maximum groove depth, and p values were further varied from 10 MPa to 5 MPa. In total, 19 experimental erosion runs were conducted (Table 1), followed by depth measurements. The grooves created were scanned using a MicroProf FRT optical profilometer. A scanning area of 150 × 100 mm with 100 lines and 1000 points/line was selected having a resolution of 1.5 mm and 100 μm along the length and width of the sample. Depth sensor SEN 000 03 with a vertical resolution of 100/30 nm and an accuracy of 1 μm was used. These scanned data were exported to SPIP software for measurement of the groove depths for each experimental run. Five depth measurements were made for each standoff distance for all the experimental runs for plotting of error bars and maximizing the statistical correctness of the experiments.

A TESCAN MIRA 3 GME scanning electron microscope (SEM) was used to observe the surface morphology of the erosion characteristics of the grooves created by the action of PWJ for different technological parameters. The sample was coated by a gold layer to make it conductive, using a rotary pump coater with an argon vacuum. The SEM was used with an accelerating voltage of 10 kV in DEPTH mode with a working distance of 50 mm using a secondary electron detector.

3 Results and discussion

A piezoelectric ultrasonic transducer operates at two frequencies, namely, resonance and anti-resonance frequency, depending upon its application. In the anti-resonance frequency mode, maximum vibration amplitude is achieved and is commonly used for ultrasonic welding, ultrasonic scalpels, and die polishers [31]. In contrast, resonance frequency shows lowest impedance and delivers maximum vibrational force. This mode of operation is used for cavitation purposes and cleaning equipment [32]. A piezoelectric ultrasonic transducer also shows maximum transmission efficiency in converting electrical energy into mechanical energy during its operation at resonance frequency. The resonance frequency is affected by variation in environmental and structural changes which lowers its transmission efficiency [33]. Commonly, ultrasonic transducers with various shapes and lengths are designed and

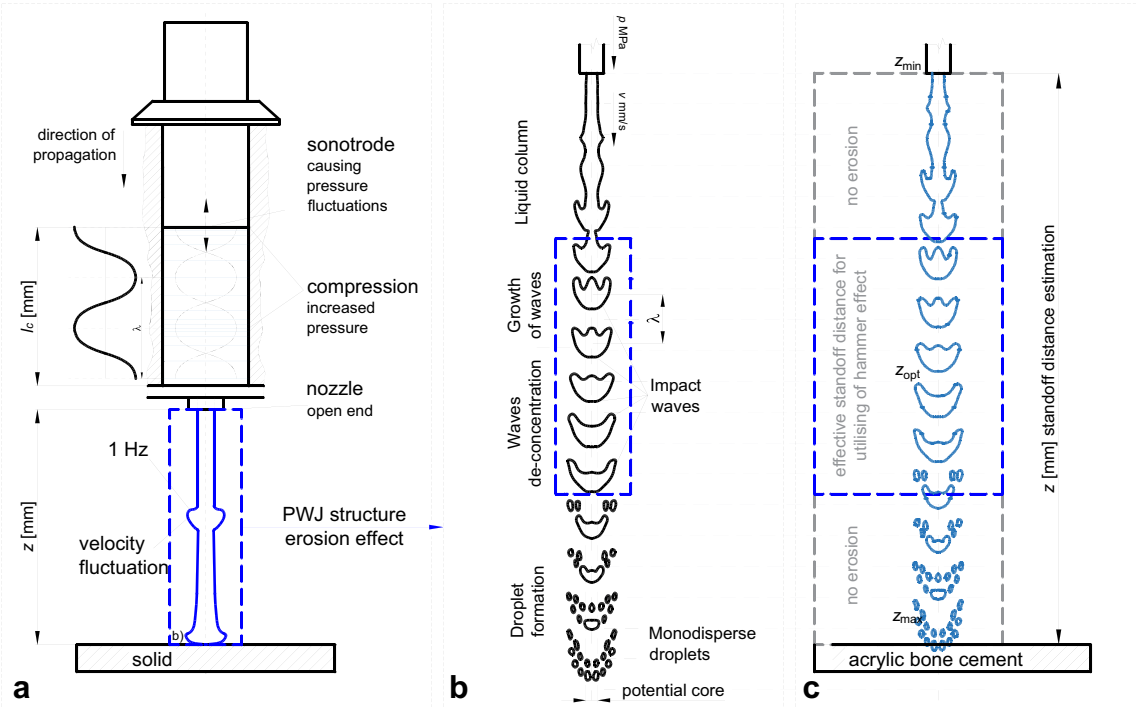

Fig. 3 Experimental set-up of utilizing ultrasonic pulsating water jet structure for maximal erosion of the acrylic bone cement, (**a**) depending on acoustic chamber length l_c [mm], (**b**) fortified water jet structure breakdown parametrically defined, (**c**) hypothesized erosion effect using minimal technological conditions

Table 1 Technological parameters

Run no.	Chamber length (l_c) [mm]	Traverse speed (v) [mm/s]	Pressure (p) [MPa]	Standoff distance (z) [mm]	Nozzle diameter (d) [mm]	Material	Theoretical volume flow rate Q [L/min]
1	0	2	10	2–20	0.3	Palacos R+G bone cement	0.54
2	2						
3	4						
4	6						
5	8						
6	10						
7	12						
8	14						
9	16						
10	18						
11	20						
12	22						
13	22	1	10				
14		0.5					
15	22	0.5	9				0.51
16			8				0.48
17			7				0.45
18			6				0.42
19			5				0.38

tested in air medium while determining their resonance frequency based on impedance curves [34]. However, when these ultrasonic transducers are used to propagate vibrations through water medium, the water load termed as water impedance affects the resonance frequency and power transmission of ultrasonic systems [35].

In PWJ, the ultrasonic sonotrode transfers mechanical vibrations into pressurized liquid entering into the acoustic chamber. These vibrations create forced decay of the jet, resulting in the formation of water droplets which impact the material surface. Therefore, for efficient utilization of ultrasonic energy, the PWJ system should be tuned to operate at resonance frequency with maximum power output. The pressurized liquid inside the acoustic chamber can be also considered as a water sonotrode which transmits and amplifies the amplitude of standing waves toward the nozzle exit. The variation of the l_c varies the volume of fluid inside the chamber, leading to variation in water impedance. Figure 4 shows the variation of f_o of the system with increasing l_c from 0 mm to 22 mm. The drop in the f_o from the f_i correlates with research

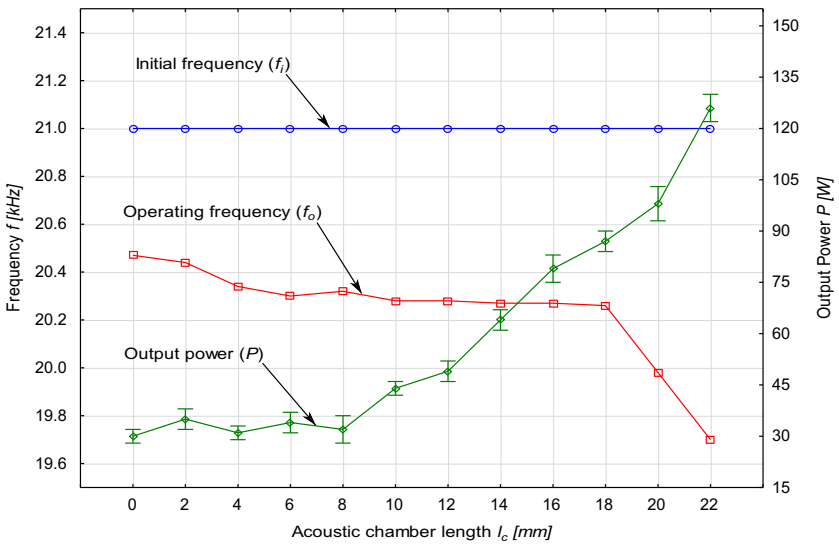

Fig. 4 Variation of f_o and P with increasing l_c from 0 to 22 mm

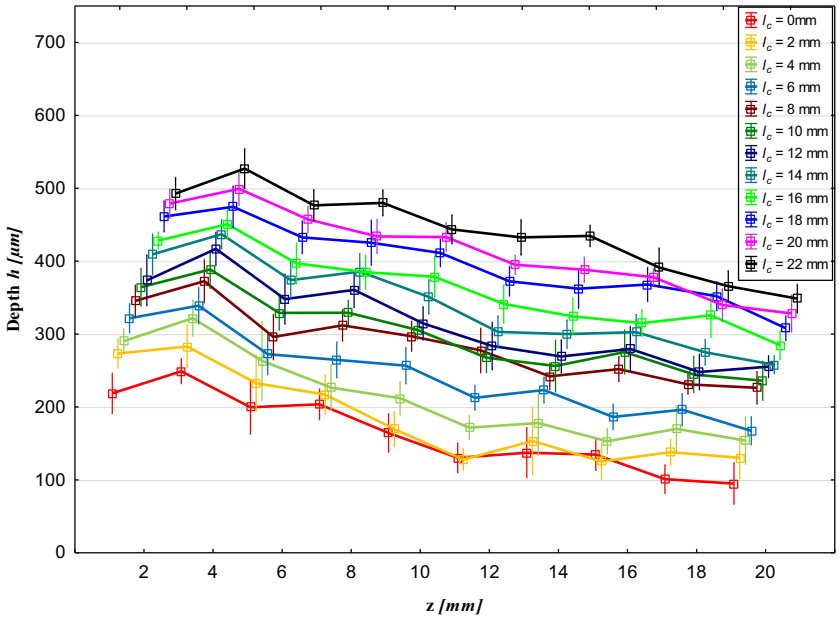

Fig. 5 Influence of acoustic chamber length (l_c = 0 to 22 mm) and standoff distance (z = 2 to 20 mm) on groove depth (h) at v = 2 mm/s and p = 10 MPa

work in which resonance frequency is found to be the lowest frequency within the impedance curve [36]. The output power of the system gradually increases with l_c due to its approach near resonance frequency, which allows efficient transmission of the ultrasonic power to the material. The output power of the system also increases at resonance frequency due to increase in current density with decrease in impedance value [33]. At l_c = 22 mm, the lowest f_o = 19.70 kHz was recorded with the maximum power output P = 126 W. Erosion tests were conducted by varying l_c from 0 to 22 mm incrementally with a step size of 2 mm to verify the tuning of the PWJ for generating deeper grooves (h = 249 and 527 μm for l_c = 0 and 22 mm, respectively, at z = 4 mm).

The depth of the grooves formed during experimental runs 1 to 12 by varying l_c and z is plotted in Fig. 5. The graph shows that with an increase in l_c, the depth of the grooves increased gradually for all z. This trend is due to the formation of standing waves and their varying amplitude inside the acoustic chamber. The standing wave's amplitude increases near the nozzle exit due to the converging shape of the nozzle. These amplitudes at the nozzle exit for each l_c determine the axial velocity fluctuation of the jet after exiting the nozzle. Erosion of the material at a certain standoff distance depends upon the velocity of the water cluster with which the jet interacts with the material. During the experiments, it was observed that with increasing l_c, deeper disintegration grooves

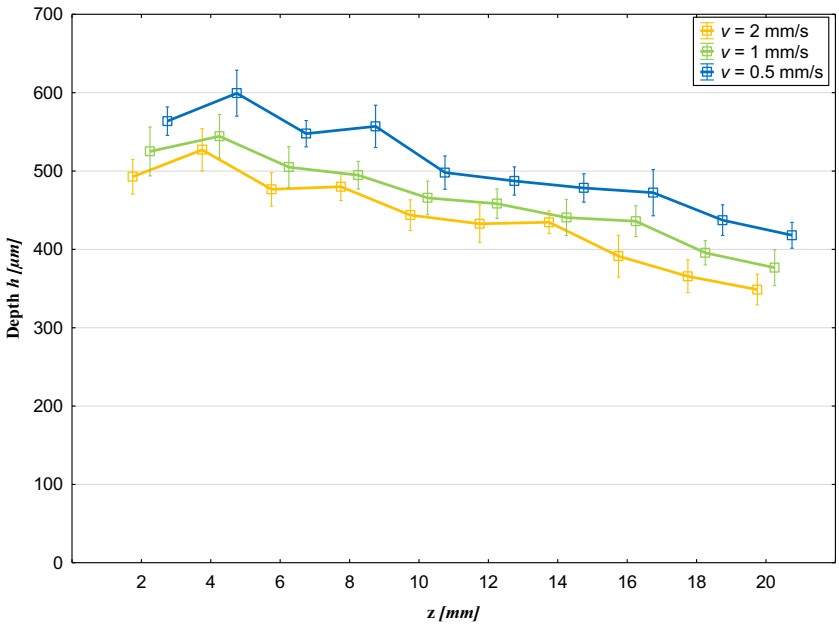

Fig. 6 Influence of traverse speed (v = 0.5 to 2 mm/s) and standoff distance (z = 2 to 20 mm) on disintegrated groove depth (h) at l_c = 22 mm and p = 10 MPa

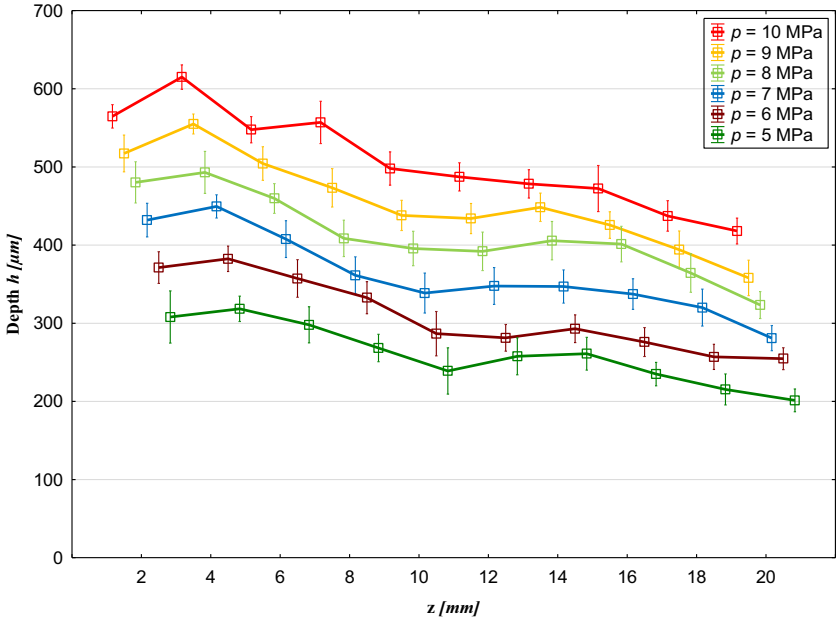

Fig. 7 Influence of water pressure (p = 5 to 10 MPa) and standoff distance (z = 2 to 20 mm) on groove depth (h) at l_c = 22 mm and v = 0.5 mm/s

were achieved (h = 249 and 322 μm for l_c = 0 and 4 mm, respectively, at z = 4 mm), which is due to the amplitude of the pressure standing wave varying from node to antinode at the nozzle exit [37]. An increase in the amplitude in turn increases the amplitude of the axial velocity with which the jet interacts with the material surface. Therefore, disintegration of the bone cement increases with increasing l_c when keeping other parameters constant. At l_c = 22 mm, greater depths were recorded for all z values as compared with the other configuration of l_c while keeping the other parameters the same (h = 249 and 527 μm for l_c = 0 and 22 mm, respectively, at z = 4 mm) (Fig. 5). With an increase in standoff distance, the distance which the water jet covers after exiting the nozzle and before interacting with the material surface increases. Increasing standoff distance increases the velocity of the water cluster, causing the jet to expand radially. Moreover, at increased standoff distance (z = 4 mm), the formation of discrete clusters of water slugs occurs, which impact the surface periodically generating the water hammer phenomenon (h = 218 and 249 μm at z = 2 and 4 mm, respectively, for l_c = 0 mm). However, with a further increase in the standoff distance after a certain limit (z = 4 mm), the aerodynamic interactions of the surrounding air with the jet increase gradually, generating a resistance toward effective disintegration. Finally, at a

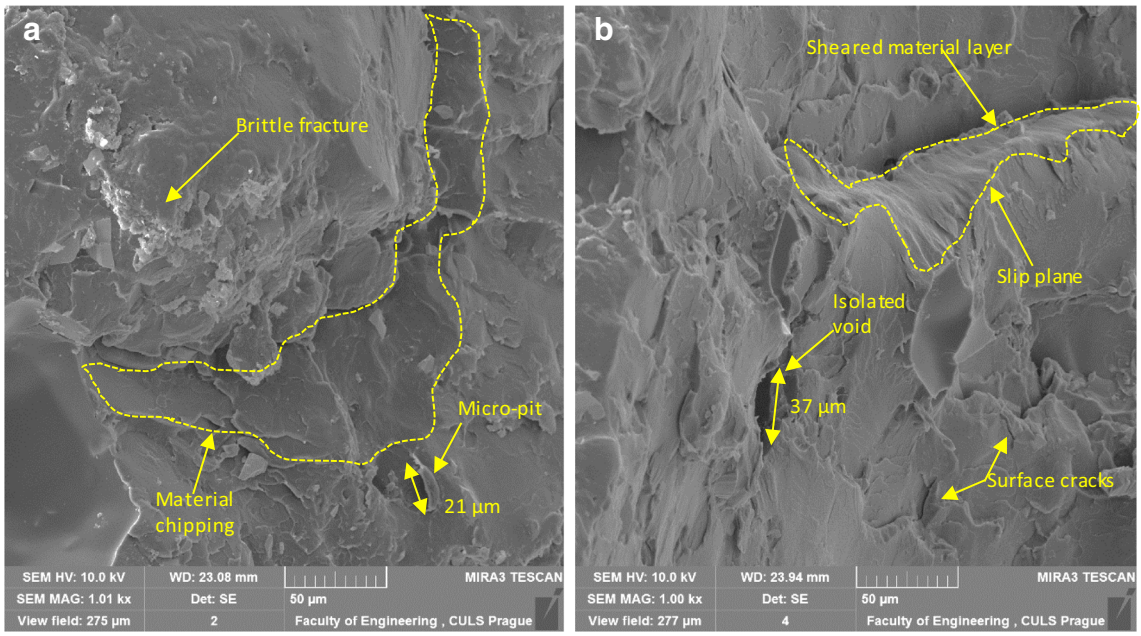

Fig. 8 SEM images of the disintegrated eroded bone cement surfaces

standoff distance of z = 20 mm, the disintegration depth is much smaller than that observed at the optimal standoff distance (h = 249 and 95 μm at z = 4 and 20 mm, respectively, for l_c = 0 mm). The determination of standoff distance range for safe and effective disintegration (z = 4 to 8 mm) will help the surgeons in the future to control the extraction of the bone cement efficiently from the femoral channel by varying the distance between the nozzle and the bone cement surface during revision arthroplasty.

Figure 6 shows the interactional influence of the traverse speed (v = 2, 1, and 0.5 mm/s) of the nozzle head with varying standoff distance (z = 0 to 20 mm). The depths of the grooves show that with a decrease in traverse speed from v = 2 to 0.5 mm/s, the number of impacts per unit length of material increases from 10,000 to 40,000 impacts/mm (operating frequency of the sonotrode f = 20 kHz). An increment in the number of impacts in turn increases the disintegration capability of the jet, resulting in greater disintegration depths [38]. The depth of the grooves increases by approximately 14% (at z = 4 mm) when compared with grooves made with v = 2 and 0.5 mm/s, keeping all other parameters constant. With a lower traverse speed, i.e., v = 0.5 mm/s, more water droplets are impacting the bone cement surface (40,000 impacts/mm) and have longer time to interact than the droplets impacting the surface at v = 2 mm/s, causing greater disintegration depths (h = 527 and 600 μm with v = 2 and 0.5 mm/s, respectively, at z = 4 mm). Moreover, in a real situation, the speed of the surgeon's hand movement during revision arthroplasty surgery is approximately comparable with 0.5 mm/s in average. The influence of the standoff distance on disintegration depth remains the same as for varying the acoustic chamber length.

Figure 7 describes the influence of the supply water pressure (p = 5 to 10 MPa) on the disintegration depth of the bone cement sample. With an increase in the pressure from p = 5 to 10 MPa, the rate of the volume of water interacting with the surface increases from 0.38 to 0.54 L/min. This increase in flow rate increases the kinetic energy of the jet, resulting in a disintegration depth of h = 615 μm for p = 10 MPa as compared with h = 318 for p = 5 MPa, at z = 4 mm. The compressive force of the water slugs impacting the surface initiates a brittle fracture of the material which penetrates further into the material due to the shear force of the water droplets interacting with the surface asperities during lateral jetting [39]. The combined stresses induced in the bone cement by the water droplets and slugs exceed the compressive strength of the bone cement (σ = 78 MPa), finally resulting in disintegration of the material by the formation of uneven grooves along the jet footprints. The influence of the standoff distance remains the same as for a change in l_c and v. The visible grooves start from the beginning, z = 2 mm, and continue till z = 20 mm. It follows a bell-shaped curve, with a maximum disintegration depth achieved after a certain standoff distance, z = 6 mm, for all pressure values and then decreases after that. In practical usage, the surgeons can regulate the supply pressure accordingly, and most of the water can be removed using suction pumps to avoid water clogging.

Surface morphology of the disintegrated bone cement was studied using SEM analysis as shown in Fig. 8. Material erosions due to brittle fractures are seen in Fig. 8a. Surface chipping at the periphery of the groove due to the lateral flow of the PWJ is observed [40]. The formation of a micro-pit is visible on the surface (Fig. 8b). These pits are formed due to the compressive forces of the jet and act as stress concentrates, which initiate crack propagation in the material [5]. The diameter of the micro-pit was measured to be approximately D = 21 μm. The sheared material layer observed in Fig. 8b is formed due to the shear forces generated during the lateral flow of the liquid. Material fracture occurs when the shear stress induced in the material exceeds the ultimate strength of the material (80 MPa). The slip plane (Fig. 8b) formed due to the sheared material layer acts as a pre-existing defect leading to compression splitting of the material. [41]. Surface cracks (Fig. 8b) are formed by the action of the repetitive impact of water slugs from the jet and further propagate by joining the surrounding micro-pits formed throughout the surface. Coalescence of these micro-pits and cracks forms surface craters and cavities. These craters and cavities lead to the formation of

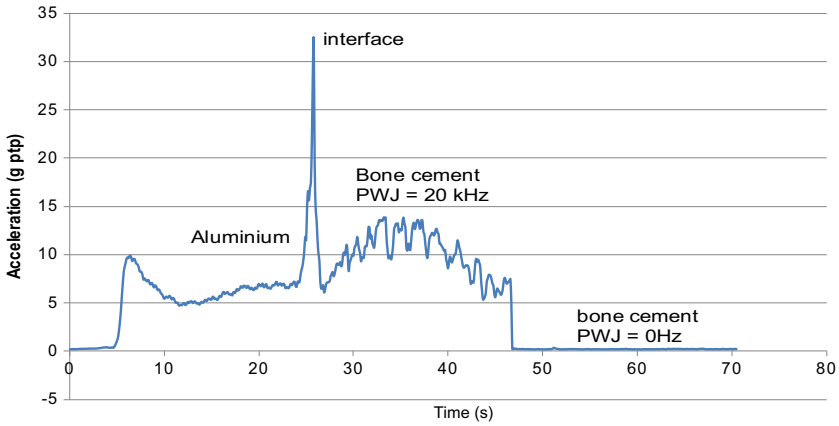

Fig. 9 On-line measurement and monitoring of PWJ interaction with bone cement clamped in aluminum matrix with evident detection of effects of continuous liquid jet (PWJ = 0 Hz) without material removal. Technological settings used: l_c = 22 mm, v = 0.5 mm/s, p = 10 MPa, and z = 4 mm

disintegrated groove-isolated voids (Fig. 8b) which are found to be created at an arbitrary distance from the central footprint of the PWJ. This is due to the constructive interference of the shockwaves traveling through the material surface, induced during the liquid–solid impact [42]. Micro-pit size measured in SEM images provides an approximate size of bone cement debris (d = 21–37 μm) created due to the impact of PWJ disintegration. In real-time application, this material debris can fall into the operative site and cause necrosis to the surrounding tissues. Therefore, an appropriate suction unit for removal of this material debris from the operative site can be designed based on the measured debris size.

Control of the disintegration process during the bone cement extraction from a single blind-hole femoral canal in revision arthroplasty procedure is required. Therefore, an on-line feedback loop control method using accelerometer sensors was tested. Vibrational signals were acquired using accelerometers placed directly on the bone cement sample during the disintegration test and processed using LabView and National Instruments (NI) software. Optimal technological settings (l_c = 22 mm, v = 0.5 mm, p = 10 MPa, and z = 4 mm) were used for the test. The jet was made to traverse from the aluminum matrix clamping the bone cement mantle to the bone cement surface to observe the changes in the acceleration signals for both materials. After 10 mm of disintegration length in bone cement, the ultrasonic system was turned off to compare its effect with continuous water jet. The time stamp of acceleration values is plotted and shown in Fig. 9. The plot shows the difference in the nature of the acceleration curve during its interaction with the aluminum matrix, at the interface and with bone cement. The acceleration values in the aluminum region are uniform due to the ductile nature of the material, where material disintegration takes place through plastic deformation and failure [43], whereas for bone cement material disintegration takes place through chipping and brittle fracture owing to the non-uniform acceleration curve [44]. Also, no acceleration values or material removal is recorded in the region impacted with continuous water jet. This depicts the advantage of using PWJ utilizing the water hammer phenomenon compared with CWJ at minimal technological conditions. On-line monitoring provides a safe method for controlling the PWJ by analyzing the response of the target material during extraction of bone cement without the risk of damaging the neighboring tissues and host bone which have different physical properties [30].

4 Conclusions

The experimental study determined the optimal working regime of PWJ in terms of z during the disintegration of bone cement. The ultrasonic system was tuned using variation in l_c for maximum power transmission (P). The interactional influence of the technological parameters such as l_c, v, and p on the morphology of the jet with varying z, leading to variation in the bone cement disintegration depth h, was studied. The major conclusions of the studies are:

1) Groove depth initially increased with increase in standoff distance to an optimal value (z = 4 mm) and then decreased with further increase in standoff length (z = 4 to 20 mm) for all experimental runs. (h = 565, 615, and 418 μm for z = 2, 4, and 20 mm, respectively, at l_c = 22 mm, v = 0.5 mm/s, and p = 10 MPa).
2) The variation of acoustic chamber length was used to tune the system for maximum utilization of input energy (P = 126 W, f_o = 19.7 kHz at l_c = 22 mm). The depth of the grooves generated increased from h = 249 to 527 μm for l_c = 0 to 22 mm, respectively, at z = 4 mm, v = 2 mm/s, and p = 10 MPa.
3) With a decrease in traverse speed from v = 2 to 0.5 mm/s, the number of impacts with the sonotrode f = 20 kHz increases from 10,000 to 40,000 impacts/mm. The increase in impacts increases the groove depth. h = 599 and 527 μm for v = 0.5 and 2 mm/s, respectively, at z = 4 mm, p = 10 MPa, and l_c = 22 mm.
4) With a decrease in the supply water pressure, the energy of the PWJ decreases, which leads to a decrease in the disintegration depth of the grooves created. For p = 10 and 5 MPa, h = 615 and 319 μm, respectively, at z = 4 mm, v = 0.5 mm/s, and l_c = 22 mm.
5) The surface morphology of the eroded bone cement surface was observed using SEM analysis. The surface images showed brittle fractured erosion features such as material chipping, micro-pits (d = 21 μm), surface cracks, isolated voids (D = 37 μm), and material shearing due to the repetitive water hammer impact of PWJ.
6) An on-line monitoring method showed its potential for control of PWJ based on the material response during disintegration of bone cement in a single blind-hole femoral canal. The variation in the acceleration values recorded during the process depends upon the physical properties of the material and can help to protect the neighboring tissue and bone from necrosis.

This study opens a new direction for the utilization of PWJ technology for minimally invasive revision arthroplasty surgeries for the extraction of bone cement. The jet morphology of the PWJ provides a safe working limit without requiring visual access within the optimal standoff distance. This technique of bone cement removal would overcome the shortcomings and limitations encountered by the current methods of cement extraction using mechanical tools. Research using physiological saline as a working fluid should be tested for its better biocompatibility properties as compared with water.

Acknowledgments Authors are thankful to Dr. Monika Hromasová for providing SEM analysis.

Funding information This study was supported by the Slovak Research and Development Agency under Contract No. APVV-17-0490 and VEGA 1/0096/18. The experiments were conducted with the support of the Institute of Clean Technologies for Mining and Utilization of Raw Materials for Energy Use - Sustainability Program, reg. no. LO1406, financed by the Ministry of Education, Youth and Sports of the Czech Republic, and with support for the long-term conceptual development of the research institution RVO: 68145535.

References

1. Momber AW (2004) Synergetic effects of secondary liquid drop impact and solid particle impact during hydro-abrasive erosion of brittle materials. Wear 256:1190–1195
2. Lu Y, Huang F, Liu X, Ao X (2015) On the failure pattern of sandstone impacted by high-velocity water jet. Int J Impact Eng 76:67–74
3. Haller P de (1933) Untersuchungen über die durch Kavitation hervorgerufenen Korrosionen. Schweizerische Bauzeitung
4. Bowden FP, Field JE (1964) The brittle fracture of solids by liquid impact, by solid impact, and by shock. Proc R Soc Lond A Math Phys Sci 282:331–352. https://doi.org/10.1098/rspa.1964.0236
5. Hancox NL, Brunton JH (1966) The erosion of solids by the repeated impact of liquid drops. Philos Trans R Soc Lond A, Math Phys Sci 260:121–139. https://doi.org/10.1098/rsta.1966.0036
6. Thomas GP, Brunton JH (1970) Drop impingement erosion of metals. Proc R Soc Lond A Math Phys Eng Sci 314:549–565. https://doi.org/10.1098/rspa.1970.0022
7. Nebeker EB (1981) Development of large diameter percussive jets. In: Proceedings of the 1st US Water Jet Symposium, WJTA, St. Louis, USA
8. Gensheng L, Zhonghou S, Changshan Z, Debin Z, Hongbing C (2005) Investigation and application of self-resonating cavitating water jet in petroleum engineering. Pet Sci Technol 23:1–15
9. Vijay MM (1992) Ultrasonically generated cavitating or interrupted jet
10. Wang P, Li Z, Ni H, Liu Y, Dou P (2020) Experimental study of rock breakage of an interrupted pulsed waterjet. Energy Rep 6:713–720
11. Lehocka D, Klich J, Foldyna J, Hloch S, Krolczyk JB, Carach J, Krolczyk GM (2016) Copper alloys disintegration using pulsating water jet. Measurement 82:375–383
12. Zeleňák M, Říha Z, Jandačka P (2020) Visualization and velocity analysis of a high-speed modulated water jet generated by a hydrodynamic nozzle. Measurement:107753
13. Foldyna J, Svehla B (2011) US . Patent. 2:1–5
14. Zhou Q, Li N, Chen X, Xu T, Hui S, Zhang D (2009) Analysis of water drop erosion on turbine blades based on a nonlinear liquid-solid impact model. Int J Impact Eng 36:1156–1171. https://doi.org/10.1016/j.ijimpeng.2009.02.007
15. Hloch S, Adamčík P, Nag A, Srivastava M, Čuha D, Müller M, Hromasová M, Klich J (2019) Hydrodynamic ductile erosion of aluminium by a pulsed water jet moving in an inclined trajectory. Wear 428–429:178–192. https://doi.org/10.1016/j.wear.2019.03.015
16. Tripathi R, Hloch S, Chattopadhyaya S, Klichová D, Ščučka J, Das AK (2020) Application of the pulsating and continous water jet for granite erosion. Int J Rock Mech Min Sci 126:104209
17. Foldyna J, Sitek L, Ščučka J, Martinec P, Valíček J, Páleníková K (2009) Effects of pulsating water jet impact on aluminium surface. J Mater Process Technol 209:6174–6180
18. Pochylý F, Habán V, Foldyna J, Sitek L (2007) 3D problem of pressure wave propagation in the tube with inconstant cross section. In: Proceedings of the International Congress on Ultrasonics, Vienna
19. Hloch S, Srivastava M, Nag A et al (2020) Effect of pressure of pulsating water jet moving along stair trajectory on erosion depth, surface morphology and microhardness. Wear 452–453:203278
20. Schmolke S, Pude F, Kirsch L, Honl M, Schwieger K, Krömer S (2004) Wärmeentwicklung bei der Wasser-Abrasivstrahl-Osteotomie/temperature measurements during abrasive water jet osteotomy. Biomed Tech Eng 49:18–21
21. Honl M, Rentzsch R, Müller G et al (2000) The use of water-jetting technology in prostheses revision surgery—first results of parameter studies on bone and bone cement. J Biomed Mater Res A 53:781–790
22. Honl M, Dierk O, Küster JR, Müller G, Müller V, Hille E, Morlock M (2001) Die Wasserstrahldiskotomie im mikroinvasiven Zugang-In-vitro-Testung und erste klinische Aspekte eines neuen Verfahrens. Z Orthop Ihre Grenzgeb 139:45–51
23. Dennis DA, Dingman CA, Meglan DA et al (1987) Femoral cement removal in revision total hip arthroplasty. A biomechanical analysis. Clin Orthop Relat Res:142–147
24. Schwaller CA, Elke R (2001) Cement removal with ultrasound in revision or total hip prosthesis. Orthopade 30:310–316
25. Williams CM, Kaude JV, Newman RC, Peterson JC, Thomas WC (1988) Extracorporeal shock-wave lithotripsy: long-term complications. Am J Roentgenol 150:311–315
26. Buchelt M, Kutschera H, Katterschafka T et al (1993) Ablation of polymethylmethacrylate by Ho: YAG, Nd: YAG, and Erb: YAG lasers. Lasers Surg Med 13:638–646
27. Sherk HH, Lane G, Rhodes A, Black J (1995) Carbon dioxide laser removal of polymethylmethacrylate. Clin Orthop Relat Res:67–71
28. J. Klanke, W.E. Siebert, C. Scholz, F. Dinkelaker, Histologic and scanning electron microscopic changes on cartilaginous surfaces after treatment with different lasers compared to mechanical tools, in: Laser in der Orthopädie. Thieme, Stuttgart, 1991, pp. 129–135.
29. Honl M, Rentzsch R, Schwieger K et al (2003) The water jet as a new tool for endoprosthesis revision surgery - An in vitro study on human bone and bone cement. Biomed Mater Eng 13:317–325
30. Kraaij G, Tuijthof GJM, Dankelman J, Nelissen RGHH, Valstar ER (2015) Waterjet cutting of periprosthetic interface tissue in loosened hip prostheses: an in vitro feasibility study. Med Eng Phys 37:245–250. https://doi.org/10.1016/j.medengphy.2014.12.009
31. Hloch S, Foldyna J, Sitek L et al (2013) Disintegration of bone cement by continuous and pulsating water jet. Teh Vjesn Gas 20:593–598
32. Hloch S, Foldyna J, Pude F et al (2015) Experimental in-vitro bone cements disintegration with ultrasonic pulsating water jet for revision arthroplasty | Eksperimentalna in-vitro razgradnja koštanog cementa pomoću ultrazvučnog pulzirajućeg mlaza vode za potrebe revizijske artroplastike. Teh Vjesn 22. https://doi.org/10.17559/TV-20150822145550
33. Hloch S, Nag A, Pude F, Foldyna J, Zeleňák M (2019) On-line measurement and monitoring of pulsating saline and water jet disintegration of bone cement with frequency 20 kHz. Measurement 147:106828
34. ZVEI. (2002) Ultrasonic assembly of thermoplastic mouldings and semi-finished products : recommendations on methods, construction and applications. ZVEI, Frankfurt am Main
35. APC International L (2002) Piezoelectric ceramics: principles and applications. APC International
36. Davari P, Ghasemi N, Zare F (2014) Power converters design and analysis for high power piezoelectric ultrasonic transducers. In:

2014 16th European Conference on Power Electronics and Applications. IEEE, pp 1–9
37. Chilibon I (2002) Underwater flextensional piezoceramic sandwich transducer. Sensors Actuators A Phys 100:287–292
38. Wevers M, Lafaut J-P, Baert L, Chilibon I (2005) Low-frequency ultrasonic piezoceramic sandwich transducer. Sensors Actuators A Phys 122:284–289
39. Gururaja TR, Schulze WA, Cross LE, Newnham RE, Auld BA, Wang YJ (1985) Piezoelectric composite materials for ultrasonic transducer applications. Part I: Resonant modes of vibration of PZT rod-polymer composites. IEEE Trans Son Ultrason 32:481–498
40. Nag A, Hloch S, Čuha D, Dixit AR, Tozan H, Petrů J, Hromasová M, Müller M (2019) Acoustic chamber length performance analysis in ultrasonic pulsating water jet erosion of ductile material. J Manuf Process 47:347–356
41. Raj P, Hloch S, Tripathi R, Srivastava M, Nag A, Klichová D, Klich J, Hromasová M, Muller M, Miloslav L, Chattopadhyaya S, Adamcik P (2019) Investigation of sandstone erosion by continuous and pulsed water jets. J Manuf Process 42:121–130. https://doi.org/10.1016/j.jmapro.2019.04.035
42. Srivastava M, Hloch S, Krejci L, Chattopadhyaya S, Dixit AR, Foldyna J (2018) Residual stress and surface properties of stainless steel welded joints induced by ultrasonic pulsed water jet peening. Meas J Int Meas Confed 127:453–462. https://doi.org/10.1016/j.measurement.2018.06.012
43. Thomas GP, Brunton JH (1970) Drop impingement erosion of metals. In: Proc. R. Soc. Lond. A. The Royal Society, pp 549–565
44. Östlund F, Howie PR, Ghisleni R, Korte S, Leifer K, Clegg WJ, Michler J (2011) Ductile–brittle transition in micropillar compression of GaAs at room temperature. Philos Mag 91:1190–1199